Tribology International 165 (2022) 107277

Contents lists available at ScienceDirect

Tribology International

journal homepage: www.elsevier.com/locate/triboint

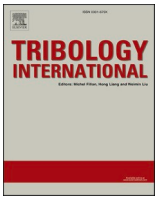

Improvement of the thermal conductivity and tribological properties of polyethylene by incorporating functionalized boron nitride nanosheets

Md Golam Rasul [a], Alper Kiziltas [b], Md Shafkat Bin Hoque [c], Arnob Banik [d], Patrick E. Hopkins [c,e,f], Kwek-Tze Tan [d], Babak Arfaei [g,*], Reza Shahbazian-Yassar [a,*]

[a] Mechanical and Industrial Engineering Department, University of Illinois at Chicago, Chicago, IL 60607, USA
[b] Research and Innovation Center, Ford Motor Company, Dearborn, MI 48124, USA
[c] Department of Mechanical and Aerospace Engineering, University of Virginia, Charlottesville, VA 22904, USA
[d] Department of Mechanical Engineering, The University of Akron, Akron, OH 44325, USA
[e] Department of Materials Science and Engineering, University of Virginia, Charlottesville, VA 22904, USA
[f] Department of Physics, University of Virginia, Charlottesville, VA 22904, USA
[g] Research and Advanced Engineering, Ford Motor Company, Palo Alto, CA 94304, USA

ARTICLE INFO

Keywords:
Boron nitride nanosheets
Thermal conductivity
Thermal distribution
Tribological properties

ABSTRACT

The heat generated by friction and wear between contact surfaces is detrimental to the performance of polymeric materials due to the low thermal conductivity of polymer materials. This work presents the effect of boron nitride (BN) nanosheets on the thermal and tribological properties of polyethylene (PE) materials. The molecular interaction between BN nanosheets and PE matrix was enhanced by functionalizing BN nanosheets with silane functional groups. It was observed that adding just *5 wt%* silane modified BN (sBN) nanosheets can increase the thermal conductivity of PE materials by *33%* and minimizes the generation of hot spots due to fast heat dissipation. In addition, the wear rate is reduced by *35%* in PE-sBN composites in comparison to PE materials.

1. Introduction

Polymer materials such as polyethylene (PE) often show poor wear and friction properties [1,2]. Such low performance can be attributed to several factors, including (i) high coefficient of friction (COF) [3], (ii) low mechanical properties [4], and (iii) low thermal conductivity of polymers leading to heat buildup during friction or wear [5]. The thermal conductivity of polymer materials plays a critical role in reducing concentrated heat generation and improving tribological properties. In fact, the poor thermal and tribological properties of polymer materials are the primary reasons for about *80%* of moving components failure and *33%* of the primary energy consumption from wear each year [6]. Since polymer materials with low mechanical properties often undergo deformation during friction, the buildup heat can lead to polymer softening, and thus, triggering a greater degree of mechanical damage and wear loss [7,8]. This deficiency has limited the applications of the polymer materials in wear-resistant applications [9].

The incorporation of nanofillers into polymers is a promising strategy to reduce wear losses [10–12]. The combination of reinforcing nanofillers and solid lubricants could reduce the wear and friction through tribofilm formation at the rubbing interfaces [6,13]. For instance, just *2 wt%* boron nitride (BN) nanosheets incorporation into polyimide (PI) nanocomposites showed *83%* reduction in wear rate and 17% reduction in COF at a low loading of nanosheets [14]. In another study, *0.5 wt%* BN nanosheets in epoxy composites led to an increase in mechanical strength and tensile modulus while reducing the wear rate by *33%* [15]. Molecular dynamics (MD) simulation also confirmed that the reinforcement of polymer with nanofillers could increase Young's modulus and shear modulus by *150%* and *27.6%*, respectively, and reducing the average COF by *35%* and abrasion rate by *48%* [16].

Interestingly, the correlation between the thermal conductivity of polymers and their tribological properties is less studied. For example, Dong and co-workers [17] coated aluminum foam/polyoxymethylene (AF/POM) composites surface by modified graphene nanomaterials. Incorporation of *5 wt%* modified graphene coating on the AF/POM composite surface increased thermal conductivity by *92%*, resulting in an improved thermal distribution of the heat generated by the friction. As a result, COF and wear loss of the coated AF/POM composites were decreased by *8* and *28%*, respectively. In another study, *55%* increase in thermal conductivity and *15%* reduction in average COF were reported

* Corresponding authors.
E-mail addresses: barfaei@ford.com (B. Arfaei), rsyassar@uic.edu (R. Shahbazian-Yassar).

https://doi.org/10.1016/j.triboint.2021.107277
Received 19 June 2021; Received in revised form 28 August 2021; Accepted 8 September 2021
Available online 12 September 2021

for incorporating *4 wt%* graphene materials into lubricant (e.g., grease) [18]. Compared to coating and lubricant techniques, polymer nanocomposites are cheaper and easily produced in bulk. Surprisingly, there is very limited study of such correlation between thermal conductivity and tribological properties for polymer nanocomposites materials. As for example, Mu and co-workers [5] showed that incorporating graphene into the polyimide resulted in a drop in contact surface temperature from *217* to *207* ℃ and reduced wear rates from 0.87×10^{-9} to 0.5×10^{-9} $cm^3N^{-1}m^{-1}$. A recent publication also demonstrated the importance of increased thermal conductivity to improve tribological properties of the composites [19]. This promising study calls for further investigation on the correlation between thermal conductivity and their tribology behavior in composite materials. Also, the role of interfacial chemistry between nanofillers and polymers on the tribology behavior needs further studies.

This work reports the effects of BN nanosheets on the thermal and tribological properties of polyethylene materials. Moreover, there has not been any systematic investigation between the thermal conductivity and tribological properties in polyethylene materials to the authors' knowledge. Two types of BN nanosheets, pristine and silane modified, were chosen for this study to reveal the effect of interfacial interactions between BN nanosheets and PE molecular chains on their thermal and tribological properties. The thermal properties of the polymer composites were studied by characterizing: (i) thermal conductivity using a hot-disc thermal analyzer and (ii) thermal maps using a point laser heating source. Moreover, the polymer composites were characterized for tribological properties: (i) wear rate (wear rates are calculated by measuring the volume of materials removed per unit surface area per unit force per unit distance traveled during wear process) was measured using auto-polishing experimental setup, and (ii) COF was obtained using a tribometer. After the dry sliding wear test, the samples were observed for surface topography using a laser microscope and surface morphology using a scanning electron microscope (SEM).

2. Materials and methods of polymer composite preparation

PE polymers were received from an industrial supplier, which were used to fabricate PE composites. The detailed characterization of the as-received PE samples is shown in a previous publication [20]. This PE material contains approximately *37 wt%* inorganic residues, i.e., aluminum oxide (Al_2O_3), zinc oxide (ZnO), and approximately *63 wt%* PE polymer matrix. In this study, the pristine and silane-modified BN nanosheets are used to fabricate polymer composites using a twin-screw extruder at the Ford Research and Innovation Center, MI. In addition to the characterization of pristine and silane-modified BN (sBN) nanosheets, the detailed fabrication method of preparing PE-BN composites is described in a previous study [20]. Both sBN and pristine BN (pBN) nanosheets are hexagonal crystal structures, and the average lateral sizes are *100–200 nm*. sBN nanosheets were made by functionalizing pBN nanosheets with *1–3 wt%* silane coupling agent (KH-550) using 3-aminopropyltriethoxysilane ($C_9H_{23}N_2O_3Si$, CAS: 919-30-2). Pristine BN nanosheets are denoted as pBN nanosheets, and silane functionalized BNs are denoted as sBN nanosheets throughout this paper. PE-pBN indicates that this composite is composed of PE and *5 wt%* pBN nanosheets. Similarly, PE-sBN indicates that this composite is composed of PE and *5 wt%* sBN nanosheets. Simply, PE-BN indicates that the PE-BN composite comprises PE and BN nanosheets (i.e., either pBN or sBN nanosheets).

3. Characterization

3.1. Thermal analysis

Thermal properties of samples were characterized to assess BN nanosheets and its silane functionalization effect on the PE materials. Thermal properties such as thermal conductivity and thermal mapping were measured using a hot-disk thermal analyzer apparatus and a Micro Thermal Imaging Microscope System.

3.1.1. Thermal conductivity

The samples' thermal conductivity was measured by a hot-disk thermal analyzer (TPS 3500) using a *0.88 mm* Kapton sensor. Hot-disk measurements are based on the transient plane source (TPS) technique, details of which can be found elsewhere [21,22]. The hot-disk analyzer was calibrated using two control samples: BK7 window glass and stainless steel. The measured values were 1.06 ± 0.04 and $13.9 \pm 0.54\ Wm^{-1}\ K^{-1}$, respectively, in excellent agreement with the literature [23,24]. For each specimen, five measurements were taken at multiple spots. The uncertainty associated with the thermal conductivity incorporates the standard deviation and the uncertainty of samples' heat capacity.

3.1.2. Thermal mapping

To assess the heat distribution property of samples, an Infra-red (IR) camera-enabled thermal mapping microscopy system (Micro Thermal Imaging Microscope System) was used [25]. A constant power laserof *100 mW* was used to heat the sample surface as a point heating source. An IR camera with a *20 μm* lens was placed right above the testing sample so that the surface temperature was detected instantly and continuously. The surface temperature of the samples was measured at the 30^{th} second from the start of heating.

3.2. Tribological analysis

3.2.1. Wear test

The dry sliding wear test was carried out using an auto polishing machine (Multiprep polishing system-*8"*, Allied high tech products Inc.), equipped with precision control of wear loading. The dry sliding wear test was done using a nominal load of *5 N* at a rotation speed of 0.025 ms^{-1} (*30 rpm*) for a specific duration in a condition of dry sliding friction. A schematic diagram of measuring the weight loss of samples in a dry sliding wear test is shown in Fig. 1. The wear rate of the samples is calculated in terms of volume loss per unit surface area using a modified equation as reported in the literature [26]:

$$K = \frac{\Delta m}{A \times F \times D \times \rho} \tag{1}$$

where K is the wear rate ($m^3m^{-2}N^{-1}m^{-1}$), Δm (g) is the amount of mass loss during the dry sliding wear test, A (m^2) is the contact surface area of the sample, F is the applied nominal load (N), ρ (g m^{-3}) is the density of materials, and D (m) is the distance traveled in the dry sliding wear test. This wear rate (K) that is used in this manuscript is the normalized value of the wear rate with respect to the contact surface area of the sample with abrasive-paper. Because of the experimental design, the contact surface area of all of the tested samples was slightly different. Therefore, the calculated wear rate (K) is more accurate representative wear rate of the samples, and it is important particularly for comparing the results among samples. Each of the samples was tested at least three times to ensure the repeatability of the results.

3.2.2. Coefficient of friction measurement

A load of 1 kg was kept on the dry surface of the samples. Later, the load was connected to the force sensor. Fig. 2 presents the schematic diagram of the experimental setup. A motion sensor was utilized to monitor and maintain constant velocity during the load movement on the samples. Both force sensor and motion sensor were connected to the data acquisition system, LabQuest 2. After placing the load over the sample, the load was being pulled forward by a yarn. Test results in terms of frictional force were analyzed using the software Logger Lite. Finally, COF, μ, was calculated using the equation, $\mu = F/R$, whereby F is

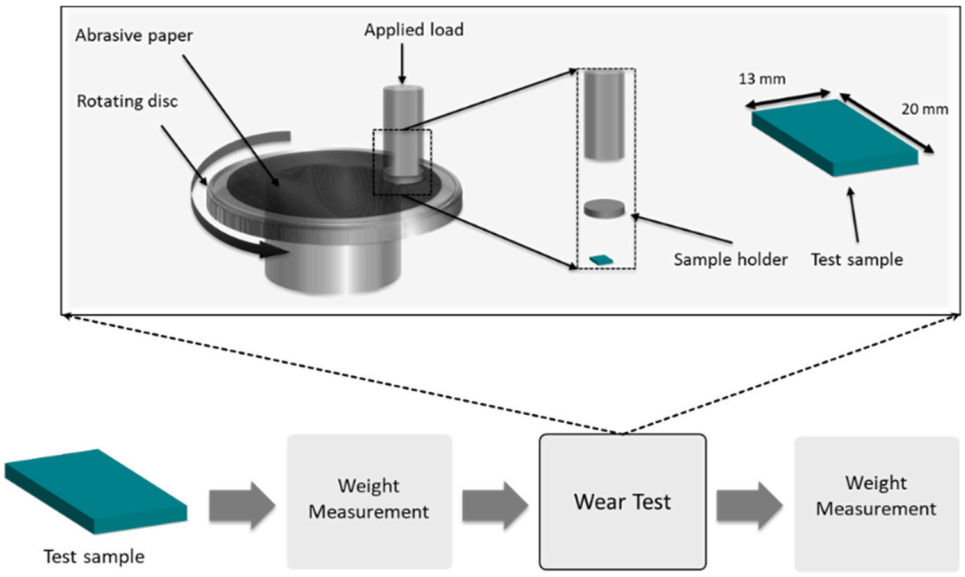

Fig. 1. Schematic diagram of an experimental set-up showing wear rate measurement of samples.

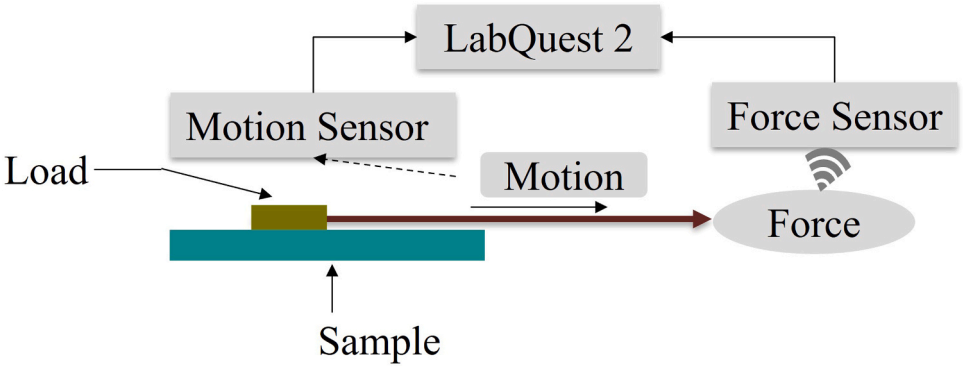

Fig. 2. Schematic diagram of an experimental set-up showing coefficient of friction measurement of samples.

the measured frictional force, and R is the reaction force, equal to the vertical load applied to the models [27]. Five trials were performed for each model to ensure experimental repeatability.

3.3. Microscopy and spectroscopy characterization

3.3.1. Optical microscopy

Three dimensional (3D) surface features were obtained to characterize the topographies of the samples. A non-contact surface profilometer (Olympus OLS5000 laser microscope) was used to collect the surface features, and Olympus OLS5000-Analysis application version 1.3.2.144 was utilized to analyze (i.e., surface features) and quantify (i.e., roughness parameters) the surface features of the samples.

3.3.2. Electron microscopy and spectroscopy analysis

Scanning electron microscope (SEM) and energy-dispersive X-ray spectroscopy (EDS) technique was utilized to visualize the surface morphology and elemental map of the samples. Samples were sputter-coated with *6.0 nm* Pt/Pd coating and imaged by JEOL JSM-IT500HR FESEM.

3.3.3. X-ray photoelectron spectroscopy (XPS)

The XPS measurements (thermo scientific ESCALAB 250Xi) were performed to detect the chemical states of the polymer materials. Avantage (surface chemical analysis) software was used to deconvolute and fit the spectra.

4. Results and discussion

In this investigation, two types of BN nanosheets, pristine and silane modified, were chosen to reveal how interfacial interactions between BN nanosheets and PE molecular chains can affect the thermal and mechanical properties of the polymer composites. This is justified knowing the poor molecular interaction between polymers and BN nanosheets [28,29]. Such weak molecular interaction is responsible for (as a contributor of) higher wear rates and interfacial thermal resistance resulting in lower thermal conductivity, as reported in numerous publications [30–32]. Therefore, increasing the molecular interaction between BN nanosheets and polymer materials is vital to improving the wear-resistant properties and thermal conductivity. Polymer-BN nanosheets molecular interaction could be improved by attaching appropriate functional groups onto BN nanosheets surface [33]. Silane functional group is an attractive choice for BN nanosheets because of the ability of increasing molecular interaction between polymers and nanofillers [34]. The silane group has organic alkyl molecules (-R), which is very compatible with the non-polar nature of the PE molecular structure (Fig. 3). The contribution of silane modification in improving PE-BN composites' properties (mechanical and thermo-mechanical) was demonstrated in our previous work [20]. Such improvement of mechanical properties (e.g., tensile modulus, strength, and shear modulus)

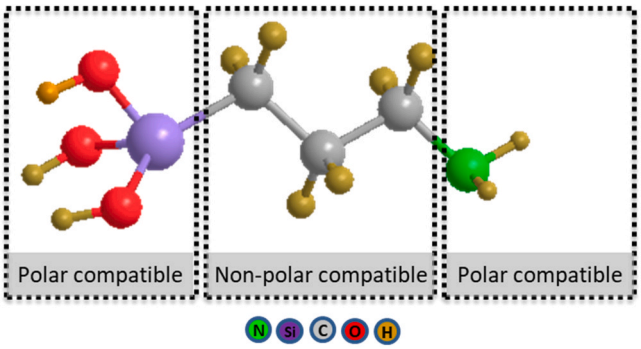

Fig. 3. Molecular structure of 3-aminopropyltriethoxy silane functional molecules (molecular formula: $C_9H_{23}N_2O_3Si$).

could further enhance the tribological performances of PE-BN composites.

4.1. Thermal analysis

The heat transport properties of PE-BN composites are evaluated by measuring the thermal conductivity, and thermal mapping test results illustrate the thermal distribution of the composites. The thermal conductivity of PE, PE-pBN (i.e., 5 wt% pBN nanosheets incorporated PE composites), and PE-sBN (i.e., 5 wt% sBN nanosheets incorporated PE composites) composites is reported in Fig. 4 to demonstrate the effect of BN nanosheets as well as silane modification on the thermal conductivity of the polymer materials. As demonstrated in Fig. 4a, the PE shows a thermal conductivity of $0.72(\pm 0.03)\ \ Wm^{-1}K^{-1}$ which is higher than the typical value of thermal conductivity in pure PE ($0.26\ \ Wm^{-1}K^{-1}$) [35]. This is because the PE used in this study was sourced from an industrial supplier containing approximately *37 wt%* of aluminum oxide (Al_2O_3) and zinc oxide (ZnO). Because of these Al_2O_3 and ZnO additives, the thermal conductivity of our PE is higher than pure PE material [36,37]. The addition of pBN nanosheets increases the thermal conductivity of PE materials from $0.72(\pm 0.03)\ \ to\ \ 0.84(\pm 0.04)\ \ Wm^{-1}K^{-1}$ which is about *17%* higher than our control PE that includes the oxide additives (i.e., Al_2O_3 and ZnO). It is likely that the BN nanosheets create thermal conductive pathways in the matrices (Fig. 4b), as shown in the SEM images of the PE-pBN and PE-sBN composites. Formation of such heat-conducting paths are also reported in published literatures where nanosheets interconnect with each other and form heat-conducting path [33,38]. On the other hand, the measured thermal conductivity of PE-sBN composites exhibits $0.96\ \ (\pm 0.06)\ \ Wm^{-1}K^{-1}$, which is *33%* higher than PE and *14%* higher than PE-pBN composites.

To demonstrate the effect of silane modification on thermal conduction process, the interfacial thermal resistances in polymer composites were calculated using the effective medium theory (EMT) [39]. According to EMT theory, thermal conductivity follows the EMT model:

$$K = k_m \frac{3 + 2V_f\left(\frac{K_p - K_m}{K_m}\right)}{3 - V_f\left[(1-\alpha) - \frac{K_m}{K_p}\right]} \tag{2}$$

and

$$\alpha = \frac{R_1 K_m}{d} \tag{3}$$

where $K_m(0.72\ Wm^{-1}K^{-1})$ is the thermal conductivity of the PE, and K_p ($300\ Wm^{-1}K^{-1}$) [40] is the thermal conductivity of the BN nanosheets filler; V_f (*0.0244*) is the volume fraction of BN nanosheets; R_1 is the interfacial thermal resistance between PE and filler; d (*50 nm*) is the thickness of BN nanosheets. The calculated value of the interfacial thermal resistance of sBN nanosheets composite is $4.12 \times 10^{-5}\ \ m^2\ WK^{-1}$, which is *15%* less than that of the pBN nanosheets composites ($4.83 \times 10^{-5}\ \ m^2\ WK^{-1}$). The reduction in interfacial thermal resistance could likely be attributed to the increased thermal conductivity of PE-sBN composites [33,41]. This indicates the importance of low interfacial thermal resistance to achieve high thermal transport properties in polymer composites. This reduction in interfacial thermal resistance is commonly observed in surface modified nanofillers incorporated polymer composites [42,43]. The increased molecular interaction between nanofillers and polymer matrices reduces interfacial thermal resistance, resulting in reduced phonon scattering [42,43]. The silane coupling agent likely acts as a bridge between the PE polymer

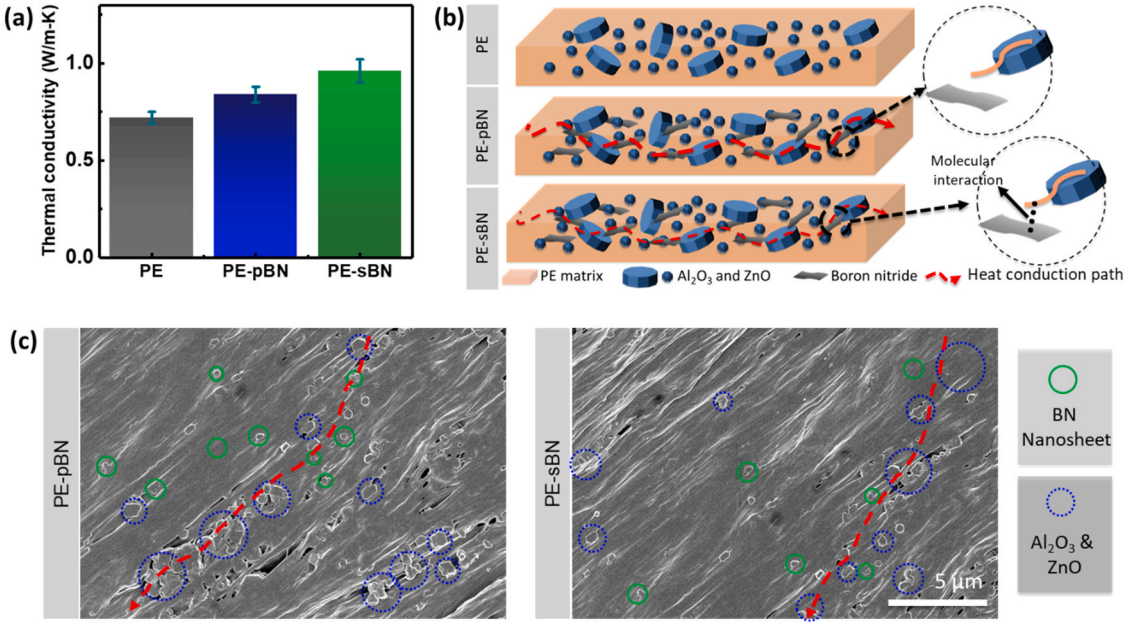

Fig. 4. Heat transport properties in PE and PE-BN composites. (a) Comparison of thermal conductivity of PE, PE-pBN, and PE-sBN composites at room temperature (*23 °C*). (b) Schematic diagram of the heat-conducting path through PE, PE-pBN, and PE-sBN composites. (c) Surface microstructures of PE-pBN and PE-sBN composites showing heat-conducting paths formation using BN nanosheets and additives (Al_2O_3 and ZnO), facilitating faster heat-conduction.

matrix and BN nanosheets, thus increasing the molecular interaction (as shown in Fig. 4b).

The thermal distribution property was evaluated by heating the samples using a point laser heating source to demonstrate the effect of thermal conductivity of materials. The point laser heating source with an input power of *100 mW* was used to illuminate the surface of the samples in a perpendicular direction. The surface temperature was recorded using an infrared (IR) camera (Fig. 5a). As shown in Fig. 5b, hot spots are formed on the sample surface. The maximum hot-spot temperature was *110 °C* for PE materials, while PE-pBN and PE-sBN composites showed *95* and *84 °C*, respectively (Fig. 5c). For PE, the hot-spot temperature is higher compared to PE-pBN and PE-sBN composites, reflecting lower thermal distribution capability. Because of the low thermal dissemination, the temperature profile of PE specimens shows that the heat is concentrated at the center and cannot be distributed through the in-plane direction of the surface (Fig. 5d). On the contrary, the temperature profiles of the PE-pBN and PE-sBN composites show a distributed profile where the surface temperature at the center is much lower than PE. At *1.5 mm* away from the hot-spot center, the surface temperature of the PE-pBN and PE-sBN composites are *39* and *36 °C* compared to *26 °C* for PE. The improved thermal distribution is likely the results of (i) the increased thermal distribution capabilities and (ii) the lower heat absorption of the PE-pBN and PE-sBN composites [44]. Such results were also reported in literature where thermal conductivity and distribution properties of polymer materials were affected by the assemblies, orientation, and surface modification of BN nanosheets [33]. For example, Cheng et al. [25] reported that aligned BN nanosheets increased the thermal conductivity of polyethylene oxide by *125%* (0.457 to 1.03 $Wm^{-1}K^{-1}$) even at a low loading of *2 wt%* BN nanosheets, resulting in a reduction of hot-spot temperatures from *389* to *295 °C*. The effect of increased molecular interaction on thermal conductivity are also demonstrated by Hou et al. [45] where thermal conductivity of epoxy-BN nanocomposites were increased from *1.04* to *1.18* $Wm^{-1}K^{-1}$ by modifying the nanofillers using coupling agent.

4.2. Tribological analysis

4.2.1. Wear rate and coefficient of friction

The tribological property of the samples was evaluated by measuring the wear rate and coefficient of friction (COF). Fig. 6a–c shows the wear rates and COFs of PE and PE-BN composites. The calculated wear rate of the PE material is about 1.33×10^{-6} $m^3m^{-2}N^{-1}m^{-1}$. The addition of pBN nanosheets reduces the wear rate to 0.99×10^{-6} $m^3m^{-2}N^{-1}m^{-1}$ which is a *26%* reduction of wear rate compared to the PE material. This reduction in wear rate indicates that the dry sliding wear test removes fewer materials from the PE-pBN composite samples compared to the PE specimens. Further, COF was measured for each of the samples, and the mean COFs are reported in Fig. 6c. The evolution of the COFs as a function of sliding time shows that the COFs of all samples are increased during the initial running-in stage (Fig. 6b). At the steady stage, the COFs are constant throughout the entire rubbing process. The PE materials indicate a high mean COF value of *0.42*. The addition of pBN nanosheets into PE reduces the COF value to *0.35*, which is *17%* reduction compared to the PE specimens. The lower COF of PE-pBN means less friction at the interface of the sliding surfaces resulting in a reduced amount of wear rate. This is in agreement with other reports [46,47]. The other possible reasons for the reduction in wear rate and COF could be explained by the following positive effects of pBN nanosheets. First, the load-carrying capability of BN nanosheets is much higher than the PE matrix. As a result, most of the wear load could be carried out by BN nanosheets during the sliding process leading to a better wear resistance [6]. The second reason for improved tribological properties could be attributed to the increased mechanical properties of PE-pBN composites. The PE matrix is mainly assembled by weak van der Waals forces between soft PE molecular segments, which could easily be deformed mechanically during friction. As reported in our previously published article [20], adding pBN nanosheets into PE increased the tensile strength and modulus. As a result, the resistance to mechanical deformation is increased, resulting in improved wear resistance of the PE-pBN composites. The third reason is related to the improved thermal conductivity and heat distribution properties of pBN nanosheets composites. The contact surface temperature increases due to frictional heat accumulation during the wearing process at the interfaces [19]. Thus, the accumulated frictional heat induces thermo-mechanical deformation, consequently, affects the wear responses. The heat generated during the wear process cannot be distributed easily due to the lower thermal conductivity of PE material. As a result, accumulated heat can soften the materials and degrade the mechanical properties. On the other hand, the increased thermal conductivity of PE-pBN composite can distribute the frictional heat and reduces the hot-spot temperature generated from the frictional heat accumulation. Thus, frictional heat accumulation is decreased, thereby reducing material degradation. While this work provides adequate insight on the role of thermal conductivity for frictional heat produced during the tribological processes, it would be interesting to study the temperature of the wear surfaces during the rubbing process using advanced techniques.

To understand the effects of silane modification of BN nanosheets on the wear response of the composites, the wear properties (wear rate and

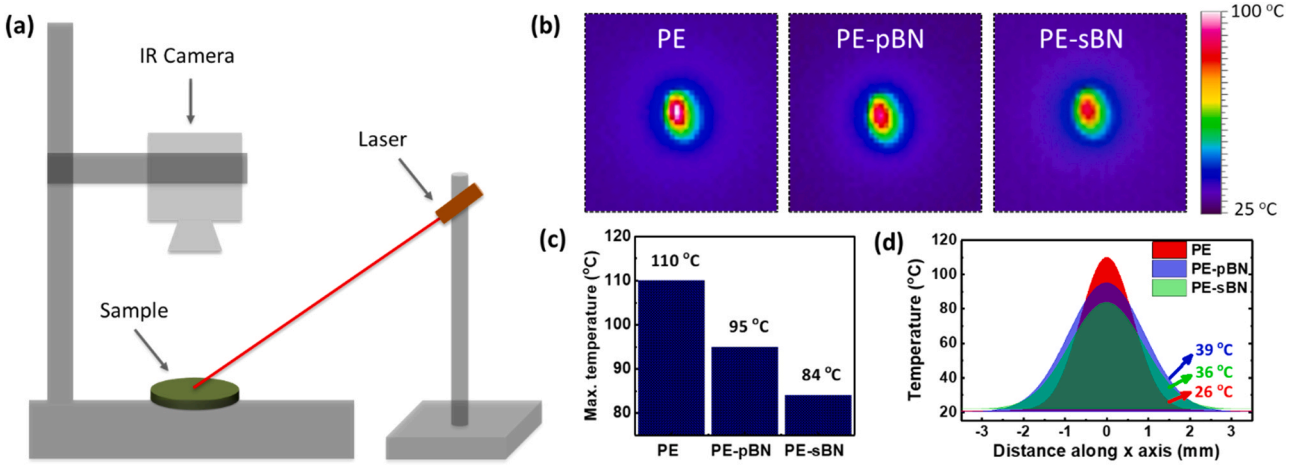

Fig. 5. Thermal distribution properties of PE and PE-BN composites. (a) Schematic diagram of thermal mapping test setup for measuring thermal mapping using point laser heating source. (b) Infrared images of the PE, PE-pBN, and PE-sBN composites when heated by a laser with a 100 mW power source. (c) The maximum hot-spot temperature of the samples is measured in (b). (d) The temperature profile of (b) samples.

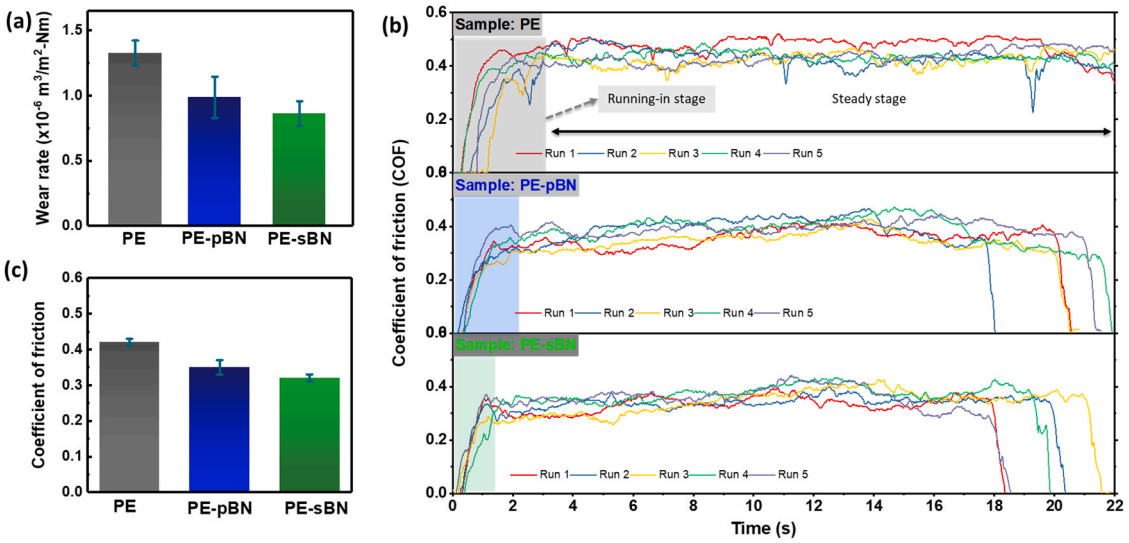

Fig. 6. Tribological properties of PE and PE-BN composites. (a) The wear rates of PE, PE-pBN, and PE-sBN composites for a wear duration of *30 min*. (b) Friction-time curves of PE, PE-pBN, and PE-sBN composites. (c) The comparison of mean coefficients of friction for PE, PE-pBN, and PE-sBN composites.

COF) of PE-sBN composites are further measured and compared to the pBN nanosheets composites. For PE-sBN composites, the wear rate and COF are measured as $0.86 \times 10^{-6}\ m^3m^{-2}N^{-1}m^{-1}$ and *0.32*, which are *35* and *24%* reductions compared to PE, respectively (Fig. 6a–c). Interestingly, the silane modification of BN nanosheets reduces the wear rate and COF by *12* and *9%* compared to pBN nanosheets composites. It is likely that the enhanced interfacial interaction between the sBN nanosheets and the PE, as reported in our earlier research article [20], is attributed to the improved wear performance of the PE-sBN composites. Because of poor interfacial interactions between polymer matrix and nanofillers, as reported in numerous literature, interfacial thermal resistance could be increased, and wear load transfer efficiency could be decreased, resulting in limited thermal conductivity and tribological properties improvement [10,48]. For instance, the effect of coupling agent was investigated for the polyimide 6,6 (PA6,6) polymer matrix where COF and wear rate were decreased by *20* and *85%*, respectively, because of the improved interfacial adhesion of 1,4-phenylene-bis-oxazoline (PBO) coupling agent [49]. In addition, wear track analysis also confirmed the reinforced effect of the PBO coupling agent on the smooth scratched surfaces.

4.2.2. *Observation of scratched surface*

Tribological properties are further illustrated by observing and analyzing the surface morphology and features (height and depth profile) after the wear process. Fig. 7 illustrates the topographies and surface morphologies of scratched surfaces after a single revolution of the wear process. As shown in Fig. 7a–b, the scratched surface of the PE is much rougher, and the roughness parameter (R_q) is measured to be *8.45 μm*. The scratched surface is composed of adhesive pits, flake areas, and large-plowed grooves. Besides, the scratched surface experiences plastic deformation and plastic flow in the process of dry sliding wear testing. When the friction force is higher than the shear resistance of the material, the molecular chain of PE is broken, resulting in debris particles on the frictional surface [1,50,51]. The debris particles are transferred and removed, which show typical adhesive wear. In contrast, the surfaces of the PE-BN composites are much smoother than PE (Fig. 7a). The calculated roughness parameter (R_q) of PE-pBN and PE-sBN composites are *3.49* and *1.06 μm*, respectively. This indicates that the degree of wearing is much less compared to PE, likely because of the increased modulus and strength of PE-BN compared to PE [20].

A single-line scratch was observed and analyzed to illustrate the tribological properties further. As shown in Fig. 8a-c, wear depth (penetration depth) decreases slightly with the addition of BN nanosheets, showing the benefits of BN nanosheets reinforcement. Significant changes are observed for the amount of debris materials piled up around the wear tracks (Fig. 8b). For PE, the debris materials are piled-up along the wear tracks and accumulated to a height of *38 μm*, as observed in Fig. 8b. In contrast, PE-BN composite shows less debris particles around

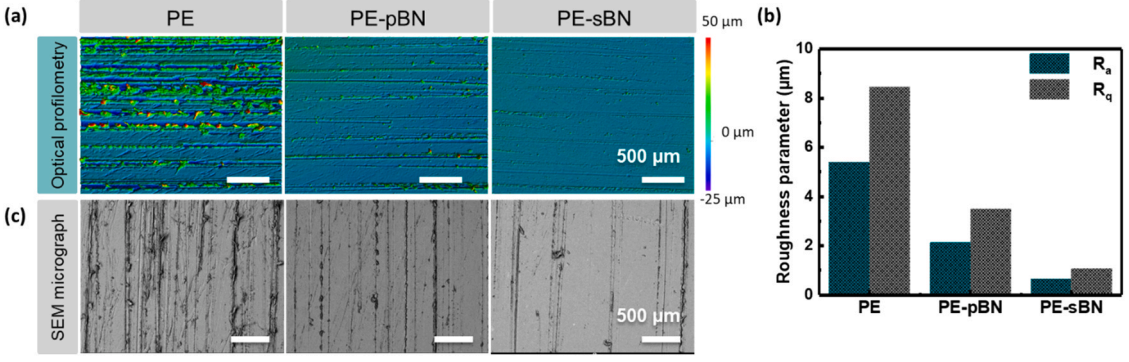

Fig. 7. Scratched surface topography and morphology of PE and PE-BN composites after one revolution of wear test using an optical profilometer and electron microscopy. (a) Laser microscopy images of PE, PE-pBN, and PE-sBN composites showing scratched surfaces. (b) The surface roughness parameters (average roughness, R_a and root mean square roughness, R_q) of PE, PE-pBN, and PE-sBN composites. (c) SEM micrograph of PE, PE-pBN, and PE-sBN composites showing worn surfaces. All scale bars in (b) and (c) have the same dimension, *500 μm*.

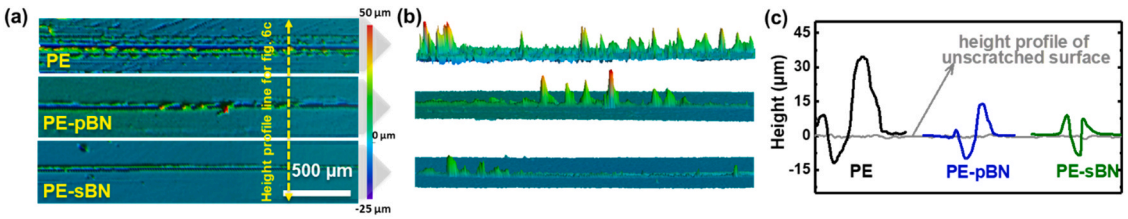

Fig. 8. Three-dimensional surface topographies and cross-sectional 3D depth profile of single line wear tracks of PE and PE-BN composites after one revolution of wear test. (a) Optical laser micrographs of single-line wear tracks of samples. (b) Cross-sectional 3D topographies of single-line wear tracks; (c) Depth and height profile of the single-line wear tracks along the dotted line in (a).

the wear tracks, resulting in much-reduced wear track heights (measured heights *15* and *10 μm* for pBN and sBN nanosheets composites, respectively). This reduced wear depths and wear track heights indicate that the PE-BN composites have higher hardness, resulting from the reinforcement of BN nanosheets [20]. As a result, the wear properties of PE-BN composites are improved when compared with PE.

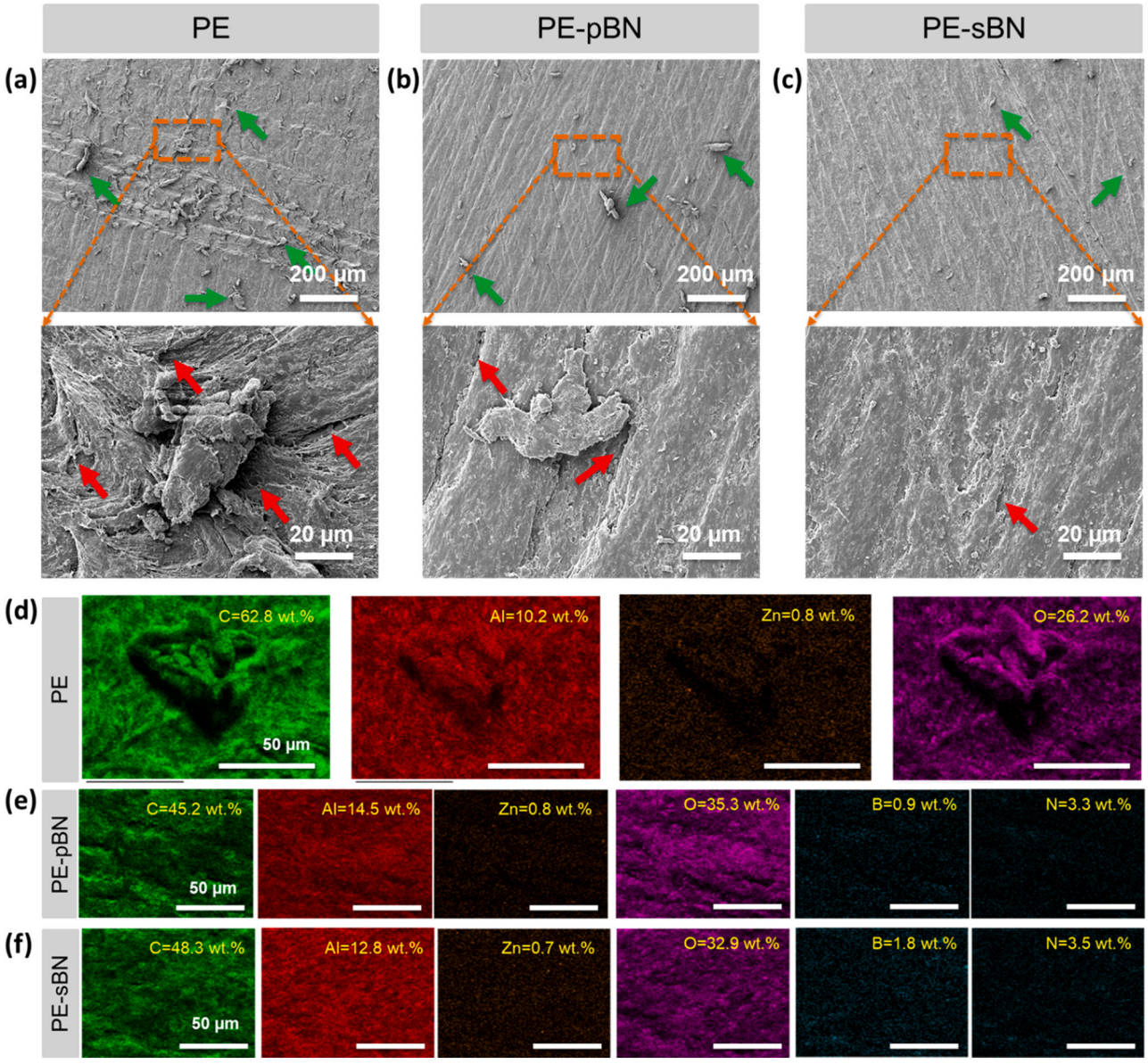

Fig. 9. Scratched surface morphology and elemental mapping of the PE and PE-BN composites after a wear test with a duration of *30 min.* (a) The large wear debris particles and wide wear tracks generated on the worn surface of PE indicate the low wear resistance of the PE materials. The smaller wear debris particles and narrower wear tracks of the scratched surfaces of PE-pBN (b) and PE-sBN (c) composites. Cavities are marked using red arrows and wear debris particles are marked using green arrows in a-c. Elemental distribution mapping of the scratched surface of (d) PE, (e) PE-pBN, and (f) PE-sBN composite materials; All scale bars in (d–f) have the same dimension, *50 μm*. (For interpretation of the references to color in this figure legend, the reader is referred to the web version of this article.)

4.2.3. Wear mechanism

The wear mechanism is further investigated by studying morphology and spectroscopy of the worn and counterpart (sand-paper) surfaces, as shown in Figs. 9 and 10. The uneven surface and severe wear tracks are observed onto the PE surface (Fig. 9a). The large wear debris particles found on the scratched surface indicate the low wear resistance of the PE. Plastic deformation was also observed on the scratched PE surface (Fig. 9a). In addition, the transfer film formed on the counterpart surface for PE, PE-pBN, and PE-sBN composites are also characterized using SEM (Fig. 10). As shown in Fig. 10a, the transfer films formed on the counterpart surface for PE are weakly attached, therefore could easily be removed and increase wear rate. This indicates that the wear process is likely governed by both adhesive and abrasive wear [52]. Contrary to the PE, the amount of wear debris of both PE-pBN and PE-sBN composite materials are found to be smaller, and wear tracks are also narrower (Fig. 9b–c). The cracks and cavities found in PE-pBN and PE-sBN composites are much smaller than PE. Moreover, the transfer film formed on the counterpart for PE-pBN and PE-sBN composites are strongly bounded (Fig. 10b–c), resulting in matrix-matrix contact. Therefore, the wear rates and COF values of PE-pBN and PE-sBN composites are lower, as evidenced from Figs. 6a and 6c. The elemental composition of the scratched surfaces was further investigated and presented in Fig. 9. There was no agglomeration of additives (i.e., Al_2O_3 and ZnO) or BN nanosheets during the wearing process. The strong oxygen signal is likely attributed to the additives (i.e., Al_2O_3 and ZnO) present in the PE polymer materials. This suggests that the wear-resistant properties of the materials are improved due to BN nanosheets' addition. It is likely that the wear process associated with PE-BN composite materials is governed by abrasive wear, as demonstrated in other literature [52].

To investigate a possible tribo-chemical reaction that could occur during wearing processes, transfer films formed on the counterpart were characterized using XPS. The XPS spectra of C 1s, Al 2p, and O 1s are observed on all samples (i.e., PE, PE-pBN, and PE-sBN composite materials), reaffirming the elemental composition (polyethylene, aluminum oxide, and zinc oxide) of the insulation-grade polyethylene polymer materials, also reported in our previous publication [20]. The B 1s spectra are present on both PE-pBN and PE-sBN composite materials, indicating the presence of BN nanosheets. The B 1s peak could be deconvoluted to B-N bonding for PE-pBN and, B-N and B-O bonding for PE-sBN composite materials, where B-O bonding is attributed to the silane functionalization of BN nanosheets [20]. Therefore, it is likely that there are no tribo-chemical reactions occurred at the contact surfaces during wearing processes.

Overall, the addition of BN nanosheets into PE polymers improves

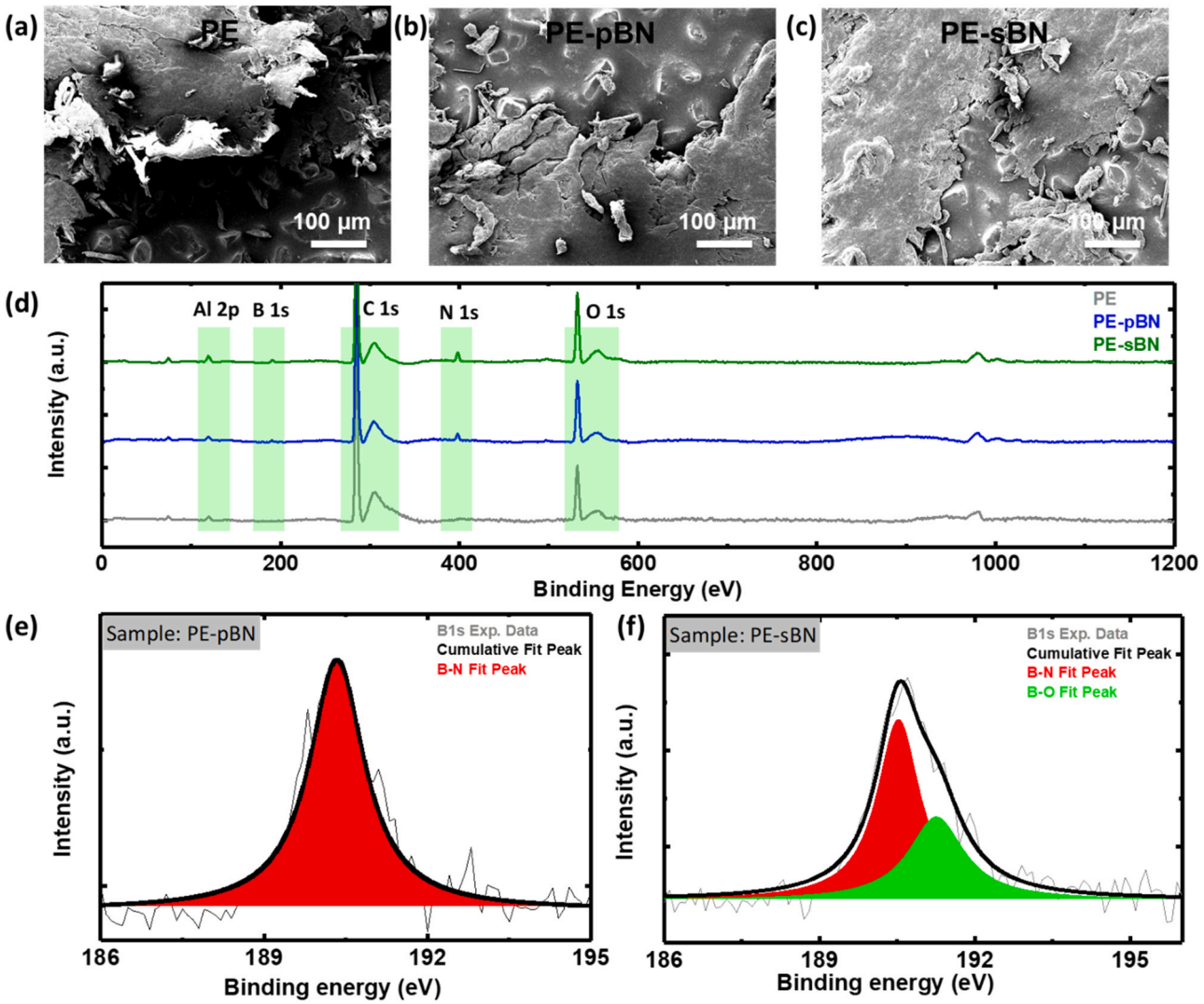

Fig. 10. Characterization of the transfer film formed on counterpart (sand-paper) for PE, PE-pBN, and PE-sBN composites after a wear test with a duration of *30 min*. The SEM images of the transfer film formed on counterpart for (a) PE, (b) PE-pBN, and (c) PE-sBN composite materials. (d) XPS survey spectra of transfer film formed on counterpart for PE, PE-pBN, and PE-sBN composite materials. Deconvoluted XPS B 1s spectrum of transfer film formed for (f) PE-pBN and (f) PE-sBN composites.

the thermal and wear-resistant properties. Such properties could further be increased with silane modification of BN nanosheets, originating from the enhanced molecular interaction between polymer matrix and silane modified BN nanosheets. The improved tribological properties are likely attributed to the enhanced mechanical properties and thermal distribution of the PE-sBN composites. The heat-conducting path, created by the additives (i.e., Al_2O_3 and ZnO) and BN nanosheets, helps reduce the heat generated by friction, thus reducing wear loss and materials' degradation during the wear process.

5. Conclusions

In summary, PE-pBN and PE-sBN composites were investigated to study the correlation between thermal and tribological properties in polymer composites. With the addition of *5 wt%* pBN and sBN nanosheets, the thermal conductivity was increased by *17* and *33%*, resulting in *14% and 23.6%* reduction of hot-spot temperature compared to the PE materials, respectively. The increased thermal conductivity of PE-sBN composites results in better thermal distribution, owing to the reduced thermal interfacial resistance. In addition, PE-pBN and PE-sBN composites demonstrated *26* and *35%* reduction in wear rate and *17* and *24%* reduction in COF, respectively, compared to the PE materials. The SEM observation revealed smoother worn surfaces of the PE-BN composites compared to the PE materials, which explains the lower COF values. On the other hand, 3D topographies of single-line scratches showed smaller wear depths and narrower wear tracks, indicating better wear resistance of PE-BN composites. Therefore, the incorporation of BN nanosheets and their silane modification significantly improve the thermal and tribological properties of the PE materials. Such polymer composites hold great potential for engineering applications, including insulation (e.g., wire insulation in automotive) and electrical components (e.g., high-voltage connectors for electric charging) where better thermal distribution and improved wear-resistant properties are demanded.

CRediT authorship contribution statement

M.G.R., **A.K.**, **B.A.**, and **R.S.Y.** initiated the idea and designed the experimental protocols. **M.G.R.** and **A.K.** compounded the nanocomposites. **M.G.R.** performed and analyzed thermal mapping, wear measurement, optical microscopy, laser microscopy, and SEM. **M.S.B.H.** and **P.E.H.** conducted the thermal conductivity measurements, and **M.G.R.** did the result analysis. **A.B.** and **K.T.T.** performed coefficient of friction test, and **M.G.R.** did the result analysis. All the authors contributed to the revision and discussion of the manuscript.

Declaration of Competing Interest

The authors declare that they have no known competing financial interests or personal relationships that could have appeared to influence the work reported in this paper.

Acknowledgements

This project is financially supported by Ford Motor Company. The fabrication of polymer composites was carried out at Ford Research and Innovation Centre, Dearborn, MI. Parts of the characterization works were carried out at the Materials Characterization and Imaging Facility (MatCI), which receives support from the MRSEC Program (NSF DMR-1720139) of the Materials Research Center at Northwestern University. M.S.B.H. and P.E.H. appreciate funding from the Office of Naval Research, Grant Number 164773-101-GG12304-31345.

References

[1] Fu H, Yan G, Li M, Wang H, Chen Y, Yan C, et al. Graphene as a nanofiller for enhancing the tribological properties and thermal conductivity of base grease. RSC Adv 2019;9:42481–8. https://doi.org/10.1039/c9ra09201c.
[2] Amirbeygi H, Khosravi H, Tohidlou E. Reinforcing effects of aminosilane-functionalized graphene on the tribological and mechanical behaviors of epoxy nanocomposites. J Appl Polym Sci 2019;136:1–8. https://doi.org/10.1002/app.47410.
[3] Friedrich K. Polymer composites for tribological applications. Adv Ind Eng Polym Res 2018;1:3–39. https://doi.org/10.1016/j.aiepr.2018.05.001.
[4] Chukov DI, Stepashkin AA, Maksimkin AV, Tcherdyntsev VV, Kaloshkin SD, Kuskov KV, et al. Investigation of structure, mechanical and tribological properties of short carbon fiber reinforced UHMWPE-matrix composites. Compos Part B Eng 2015;76:79–88. https://doi.org/10.1016/j.compositesb.2015.02.019.
[5] Mu L, Shi Y, Feng X, Zhu J, Lu X. The effect of thermal conductivity and friction coefficient on the contact temperature of polyimide composites: Experimental and finite element simulation. Tribol Int 2012;53:45–52. https://doi.org/10.1016/j.triboint.2012.04.003.
[6] Hu C, Qi H, Yu J, Zhang G, Zhang Y, He H. Significant improvement on tribological performance of polyimide composites by tuning the tribofilm nanostructures. J Mater Process Technol 2020;281:116602. https://doi.org/10.1016/j.jmatprotec.2020.116602.
[7] Xie C, Wang K. Synergistic modification of the tribological properties of polytetrafluoroethylene with polyimide and boron nitride. Friction 2020. https://doi.org/10.1007/s40544-020-0431-y.
[8] Chang L, Zhang Z, Zhang H, Schlarb AK. On the sliding wear of nanoparticle filled polyamide 66 composites. Compos Sci Technol 2006;66:3188–98. https://doi.org/10.1016/j.compscitech.2005.02.021.
[9] Stachowiak G, Batchelor A. Engineering tribology. Butterworth-Heinemann; 2006. https://doi.org/10.1016/B978-0-7506-7836-0.X5000-7.
[10] Li Y, Wang S, Wang Q. A molecular dynamics simulation study on enhancement of mechanical and tribological properties of polymer composites by introduction of graphene. Carbon N Y 2017;111:538–45. https://doi.org/10.1016/j.carbon.2016.10.039.
[11] Li Y, Wang S, Wang Q. Enhancement of tribological properties of polymer composites reinforced by functionalized graphene. Compos Part B Eng 2017;120:83–91. https://doi.org/10.1016/j.compositesb.2017.03.063.
[12] Ji Z, Zhang L, Xie G, Xu W, Guo D, Luo J, et al. Mechanical and tribological properties of nanocomposites incorporated with two-dimensional materials. Friction 2020;8:813–46. https://doi.org/10.1007/s40544-020-0401-4.
[13] Lv Y, Wang W, Xie G, Luo J. Self-lubricating PTFE-based composites with black phosphorus nanosheets. Tribol Lett 2018;66:61. https://doi.org/10.1007/s11249-018-1010-5.
[14] Min YJ, Kang KH, Kim DE. Development of polyimide films reinforced with boron nitride and boron nitride nanosheets for transparent flexible device applications. Nano Res 2018;11:2366–78. https://doi.org/10.1007/s12274-017-1856-0.
[15] Chen J, Chen B, Li J, Tong X, Zhao H, Wang L. Enhancement of mechanical and wear resistance performance in hexagonal boron nitride-reinforced epoxy nanocomposites. Polym Int 2017;66:659–64. https://doi.org/10.1002/pi.5296.
[16] Li Y, Wang S, Wang Q. A molecular dynamics simulation study on enhancement of mechanical and tribological properties of polymer composites by introduction of graphene. Carbon N Y 2017;111:538–45. https://doi.org/10.1016/j.carbon.2016.10.039.
[17] Dong P, Long C, Peng Y, Peng X, Guo F. Effect of coatings on thermal conductivity and tribological properties of aluminum foam/polyoxymethylene interpenetrating composites. J Mater Sci 2019;54:13135–46. https://doi.org/10.1007/s10853-019-03826-9.
[18] Fu H, Yan G, Li M, Wang H, Chen Y, Yan C, et al. Graphene as a nanofiller for enhancing the tribological properties and thermal conductivity of base grease. RSC Adv 2019;9:42481–8. https://doi.org/10.1039/C9RA09201C.
[19] Li P, Zhang Z, Yang M, Yuan J, Jiang W. Synchronously improved thermal conductivity and tribological performance of self-lubricating fabric liner composites via integrated design method with copper yarn. Tribol Int 2021;164:107204. https://doi.org/10.1016/j.triboint.2021.107204.
[20] Rasul MG, Kiziltas A, Malliakas CD, Rojaee R, Sharifi-Asl S, Foroozan T, et al. Polyethylene-BN nanosheets nanocomposites with enhanced thermal and mechanical properties. Compos Sci Technol 2021;204:108631. https://doi.org/10.1016/j.compscitech.2020.108631.
[21] Gustafsson SE. Transient plane source techniques for thermal conductivity and thermal diffusivity measurements of solid materials. Rev Sci Instrum 1991;62:797–804. https://doi.org/10.1063/1.1142087.
[22] Bin S, Ansari N, Khodadadi JM. International Journal of Heat and Mass Transfer Explaining the " anomalous " transient hot wire-based thermal conductivity measurements near solid-liquid phase change in terms of solid-solid transition. Int J Heat Mass Transf 2018;125:210–7. https://doi.org/10.1016/j.ijheatmasstransfer.2018.04.014.
[23] Assael MJ, Botsios S, Gialou K, Metaxa IN. Thermal conductivity of polymethyl methacrylate (PMMA) and borosilicate crown glass BK7. Int J Thermophys 2005;26(1595–605). https://doi.org/10.1007/s10765-005-8106-5.
[24] Ho, C.Y., & Chu TK. Electrical resistivity and thermal conductivity of nine selected AISI stainless steels (No. CINDAS-45); 1977.
[25] Cheng M, Ramasubramanian A, Rasul MG, Jiang Y, Yuan Y, Foroozan T, et al. Direct ink writing of polymer composite electrolytes with enhanced thermal conductivities. Adv Funct Mater 2021;31:2006683. https://doi.org/10.1002/adfm.202006683.

[26] Unal H, Mimaroglu A, Kadioglu U, Ekiz H. Sliding friction and wear behaviour of polytetrafluoroethylene and its composites under dry conditions. Mater Des 2004; 25:239–45. https://doi.org/10.1016/j.matdes.2003.10.009.
[27] Banik A, Tan KT. Dynamic friction performance of hierarchical biomimetic surface pattern inspired by frog toe-pad. Adv Mater Interfaces 2020;7:2000987. https://doi.org/10.1002/admi.202000987.
[28] Chen S, Xu R, Liu J, Zou X, Qiu L, Kang F, et al. Simultaneous production and functionalization of boron nitride nanosheets by sugar-assisted mechanochemical exfoliation. Adv Mater 2019;31:1804810. https://doi.org/10.1002/adma.201804810.
[29] Kumari S, Sharma OP, Gusain R, Mungse HP, Kukrety A, Kumar N, et al. Alkyl-chain-grafted hexagonal boron nitride nanoplatelets as oil-dispersible additives for friction and wear reduction. ACS Appl Mater Interfaces 2015;7:3708–16. https://doi.org/10.1021/am5083232.
[30] Yu J, Huang X, Wu C, Wu X, Wang G, Jiang P. Interfacial modification of boron nitride nanoplatelets for epoxy composites with improved thermal properties. Polymer 2012;53:471–80. https://doi.org/10.1016/j.polymer.2011.12.040.
[31] Li S, Duan C, Li X, Shao M, Qu C, Zhang D, et al. The effect of different layered materials on the tribological properties of PTFE composites. Friction 2020;8: 542–52. https://doi.org/10.1007/s40544-019-0276-4.
[32] Gao F, Kotvis PV, Tysoe WT. The surface and tribological chemistry of chlorine- and sulfur-containing lubricant additives. Tribol Int 2004;37:87–92. https://doi.org/10.1016/S0301-679X(03)00040-9.
[33] Rasul MG, Kiziltas A, Arfaei B, Shahbazian-Yassar R. 2D boron nitride nanosheets for polymer composite materials. Npj 2D Mater Appl 2021;5:56. https://doi.org/10.1038/s41699-021-00231-2.
[34] Chaffin K, Taylor C. TG. 14-Bonding strategies and adhesives for joining medical device components. Join Assem Med Mater Devices Biomater 2013:370–404. https://doi.org/10.1533/9780857096425.3.370.
[35] Zhou W, Qi S, An Q, Zhao H, Liu N. Thermal conductivity of boron nitride reinforced polyethylene composites. Mater Res Bull 2007;42:1863–73. https://doi.org/10.1016/j.materresbull.2006.11.047.
[36] Cao J, Wang H, Cao C, Li H, Xiao L, Qian Q, et al. Simultaneously enhanced mechanical properties and thermal properties of ultrahigh-molecular-weight polyethylene with polydopamine-coated α-alumina platelets. Polym Int 2019;68: 151–9. https://doi.org/10.1002/pi.5711.
[37] Zhang S, Cao XY, Ma YM, Ke YC, Zhang JK, Wang FS. The effects of particle size and content on the thermal conductivity and mechanical properties of Al_2O_3/high density polyethylene (HDPE) composites. Express Polym Lett 2011;5:581–90. https://doi.org/10.3144/expresspolymlett.2011.57.
[38] Zou D, Huang X, Zhu Y, Chen J, Jiang P. Boron nitride nanosheets endow the traditional dielectric polymer composites with advanced thermal management capability. Compos Sci Technol 2019;177:88–95. https://doi.org/10.1016/j.compscitech.2019.04.027.
[39] Nan C-W, Birringer R, Clarke DR, Gleiter H. Effective thermal conductivity of particulate composites with interfacial thermal resistance. J Appl Phys 1997;81: 6692–9. https://doi.org/10.1063/1.365209.
[40] Badgayan ND, Samanta S, Sahu SK, Siva SBV, Sadasivuni KK, Sahu D, et al. Tribological behaviour of 1D and 2D nanofiller based high densitypoly-ethylene hybrid nanocomposites: a run-in and steady state phase analysis. Wear 2017; 376–377:1379–90. https://doi.org/10.1016/j.wear.2016.12.037.
[41] He D, Cai M, Yan H, Lin Q, Fan X, Zhang L, et al. Tribological properties of $Ti_3C_2T_x$ MXene reinforced interpenetrating polymers network coating. Tribol Int 2021;163: 107196. https://doi.org/10.1016/j.triboint.2021.107196.
[42] Morishita T, Okamoto H. Facile exfoliation and noncovalent superacid functionalization of boron nitride nanosheets and their use for highly thermally conductive and electrically insulating polymer nanocomposites. ACS Appl Mater Interfaces 2016;8:27064–73. https://doi.org/10.1021/acsami.6b08404.
[43] Wu K, Fang J, Ma J, Huang R, Chai S, Chen F, et al. Achieving a collapsible, strong, and highly thermally conductive film based on oriented functionalized boron nitride nanosheets and cellulose nanofiber. ACS Appl Mater Interfaces 2017;9: 30035–45. https://doi.org/10.1021/acsami.7b08214.
[44] Li T, Song J, Zhao X, Yang Z, Pastel G, Xu S, et al. Anisotropic, lightweight, strong, and super thermally insulating nanowood with naturally aligned nanocellulose. Sci Adv 2018;4:eaar3724. https://doi.org/10.1126/sciadv.aar3724.
[45] Hou J, Li G, Yang N, Qin L, Grami ME, Zhang Q, et al. Preparation and characterization of surface modified boron nitride epoxy composites with enhanced thermal conductivity. RSC Adv 2014;4:44282–90. https://doi.org/10.1039/c4ra07394k.
[46] Wang H, Xie G, Zhu Z, Ying Z, Zeng Y. Enhanced tribological performance of the multi-layer graphene filled poly(vinyl chloride) composites. Compos Part A Appl Sci Manuf 2014;67:268–73. https://doi.org/10.1016/j.compositesa.2014.09.011.
[47] Gu D, Zhang L, Chen S, Song K, Liu S. Significant reduction of the friction and wear of PMMA Based composite by filling with PTFE. Polymers 2018;10:966. https://doi.org/10.3390/polym10090966.
[48] Shen X, Zheng Q, Kim J. Rational design of two-dimensional nanofillers for polymer nanocomposites toward multifunctional applications. Prog Mater Sci 2021;115:100708. https://doi.org/10.1016/j.pmatsci.2020.100708.
[49] Karsli NG, Yilmaz T, Gul O. Effects of coupling agent addition on the adhesive wear, frictional and thermal properties of glass fiber-reinforced polyamide 6,6 composites. Polym Bull 2018;75:4429–44. https://doi.org/10.1007/s00289-018-2278-1.
[50] Han JH, Zhang H, Chu PF, Imani A, Zhang Z. Friction and wear of high electrical conductive carbon nanotube buckypaper/epoxy composites. Compos Sci Technol 2015;114:1–10. https://doi.org/10.1016/j.compscitech.2015.03.012.
[51] Ouyang T, Shen Y, Yang R, Liang L, Liang H, Lin B, et al. 3D hierarchical porous graphene nanosheets as an efficient grease additive to reduce wear and friction under heavy-load conditions. Tribol Int 2020;144:106118. https://doi.org/10.1016/j.triboint.2019.106118.
[52] He J, Zhang L, Li C. Effect of perfluoroalkylmethacrylate ester-grafted-linear low-density polyethylene on the tribological property of polyoxymethylene-linear low-density polyethylene composites. Polym Eng Sci 2011;51:925–30. https://doi.org/10.1002/pen.21915.